PCCP

Physical Chemistry Chemical Physics

This paper is published as part of a PCCP Themed Issue on:

Nanophotonics: Plasmonics and Metal Nanoparticles

Guest Editors: Greg V. Hartland (University of Notre Dame) and Paul Mulvaney (University of Melbourne)

Editorial

Nanophotonics: plasmonics and metal nanoparticles
Phys. Chem. Chem. Phys., 2009
DOI: 10.1039/b911746f

Communication

Recombination rates for single colloidal quantum dots near a smooth metal film
Xiaohua Wu, Yugang Sun and Matthew Pelton, *Phys. Chem. Chem. Phys.*, 2009
DOI: 10.1039/b903053k

Papers

Gain and loss of propagating electromagnetic wave along a hollow silver nanorod
Haining Wang and Shengli Zou, *Phys. Chem. Chem. Phys.*, 2009
DOI: 10.1039/b901983a

Two-photon imaging of localized optical fields in the vicinity of silver nanowires using a scanning near-field optical microscope
Kohei Imura, Young Chae Kim, Seongyong Kim, Dae Hong Jeong and Hiromi Okamoto, *Phys. Chem. Chem. Phys.*, 2009
DOI: 10.1039/b904013g

Anisotropy effects on the time-resolved spectroscopy of the acoustic vibrations of nanoobjects
Aurélien Crut, Paolo Maioli, Natalia Del Fatti and Fabrice Vallée, *Phys. Chem. Chem. Phys.*, 2009
DOI: 10.1039/b902107h

Coupling to light, and transport and dissipation of energy in silver nanowires
Hristina Staleva, Sara E. Skrabalak, Christopher R. Carey, Thomas Kosel, Younan Xia and Gregory V. Hartland, *Phys. Chem. Chem. Phys.*, 2009
DOI: 10.1039/b901105f

The versatile colour gamut of coatings of plasmonic metal nanoparticles
Catherine S. Kealley, Michael B. Cortie, Abbas I. Maaroof and Xiaoda Xu, *Phys. Chem. Chem. Phys.*, 2009
DOI: 10.1039/b903318a

Probing the surface-enhanced Raman scattering properties of Au–Ag nanocages at two different excitation wavelengths
Matthew Rycenga, Kirk K. Hou, Claire M. Cobley, Andrea G. Schwartz, Pedro H. C. Camargo and Younan Xia, *Phys. Chem. Chem. Phys.*, 2009
DOI: 10.1039/b903533h

The effect of surface roughness on the plasmonic response of individual sub-micron gold spheres
Jessica Rodríguez-Fernández, Alison M. Funston, Jorge Pérez-Juste, Ramón A. Álvarez-Puebla, Luis M. Liz-Marzán and Paul Mulvaney, *Phys. Chem. Chem. Phys.*, 2009
DOI: 10.1039/b905200n

White light scattering spectroscopy and electron microscopy of laser induced melting in single gold nanorods
Peter Zijlstra, James W. M. Chon and Min Gu, *Phys. Chem. Chem. Phys.*, 2009
DOI: 10.1039/b905203h

Influence of the close sphere interaction on the surface plasmon resonance absorption peak
Carlos Pecharromán, *Phys. Chem. Chem. Phys.*, 2009
DOI: 10.1039/b902489c

White light scattering spectroscopy and electron microscopy of laser induced melting in single gold nanorods

Peter Zijlstra, James W. M. Chon* and Min Gu

Received 13th March 2009, Accepted 29th April 2009
First published as an Advance Article on the web 1st June 2009
DOI: 10.1039/b905203h

We present the first measurements of laser induced melting and reshaping of single gold nanorods. Using a combination of white light scattering spectroscopy and electron microscopy we find a melting energy of 260 fJ for nanorods with an average size of 92 × 30 nm. Contrary to previous reports on ensembles of nanorods, this melting energy corresponds well to the theoretical prediction of 225 fJ. We observe a gradual shape change from a long and thin rod to a shorter and wider rod, which eventually collapses into a sphere when enough laser energy is deposited. We also observe that higher aspect ratio particles are thermodynamically less stable, leading to a greater reduction of the aspect ratio at lower laser pulse energy densities.

Introduction

Small metal particles exhibit complex optical and physical properties. Their small sizes (<100 nm) cause strong confinement of the electrons, giving rise to fascinating effects not observed in the bulk material. Their surface plasmon resonance (SPR) induces a strong interaction with light, and the wavelength at which this resonance occurs depends on the local environment, shape, size and orientation of the particle.[1–3] Fundamental aspects and potential technological applications have been widely investigated in the past decade, and metal nanoparticles have been used for catalysis,[4,5] sub-wavelength optical devices,[6–9] surface enhanced Raman spectroscopy,[10,11] biological imaging and sensing,[12–18] optical recording[19–22] and photo-activated cancer treatment.[23–25]

The excitation of the SPR by an electromagnetic field such as laser light creates a free electron oscillation which decays through radiative and non-radiative decay channels.[26] In metal particles, non-radiative decay is prevalent and releases thermal energy through electron–phonon scattering,[27] causing an increase in particle temperature. The extent of the temperature increase depends on the laser pulse energy and the absorption cross section at the laser wavelength. Because the time constant of heat dissipation to the environment is on the order of hundreds of picoseconds,[28] the laser pulse width also plays a role in the photothermal energy conversion process.[29]

When enough photon energy is conveyed to the lattice, the particle reaches its melting temperature and undergoes a phase transition, starting at the surface.[30–36] Such surface melting occurs over a broad temperature range and involves the formation of a thin liquid layer at temperatures well below the melting point.[30–36] This melting point reduction occurs due to the surface tension difference between the liquid and solid phases.[30,31,33,35] In contrast to surface melting, the homogeneous melting of the solid core occurs abruptly at the critical melting temperature[34,36] (T_{melt} ~ 1300 K for bulk gold[37]) and involves sudden disordering of the lattice structure.[38–44] For particles <5 nm the homogeneous melting temperature is inversely proportional to the radius of the particle,[31,34,35] whereas for larger particles melting occurs near the bulk melting point. Also curvature driven surface diffusion can play a role in the melting of nanoparticles.[45,46]

Structural changes associated with melting of 2–20 nm diameter gold particles were reported by Ruan *et al.* using ultrafast electron crystallography.[42] By monitoring the peaks in the electron diffraction pattern after optical excitation, they observed reversible surface melting and full melting of the nanoparticles within the first 100 ps after excitation. Plech *et al.* used ultrafast X-ray diffraction to monitor the lattice expansion and cooling of 100 nm diameter gold nanoparticles.[44] They also observed a loss of long-range lattice order at elevated temperatures, which was attributed to pre-melting of the particles. At the bulk melting point complete melting was observed within 100 ps after excitation.

Phase transitions were also observed in the temperature dependent elastic properties of gold nanospheres. Hartland *et al.* employed pump–probe spectroscopy to monitor the femtosecond laser induced acoustic oscillations in gold nanospheres.[47] They reported a pump-laser intensity dependent breathing mode period, which was attributed to softening of the elastic properties due to laser-induced heating. No abrupt changes caused by the melting transition were observed, probably due to the limited increase in particle temperature due to absorption saturation. In 2007 Plech *et al.* reported a comparable technique, in which the nanoparticles were continuously heated with a resistive heater.[48] They found a sudden change in the phase and damping time of the breathing mode when the 60 nm diameter particles were heated to above 104 °C, which was attributed to the onset of surface melting below the bulk melting point.

The timescale on which the nanoparticles are heated plays a critical role in the melting process. Link *et al.* showed that reshaping of gold nanorods occurs at lower pulse energy for

Centre for Micro-Photonics, Faculty of Engineering and Industrial Sciences, Swinburne University of Technology, P. O. Box 218, Hawthorn, 3122, VIC, Australia.
E-mail: JChon@groupwise.swin.edu.au

femtosecond laser pulses compared to nanosecond laser pulses.[29] This was interpreted as an effect of energy loss to the environment during the course of the nanosecond laser pulse. In 2006 Petrova *et al.* studied the melting of gold nanorods under continuous heating, and compared these results to femtosecond laser induced melting.[49] Under laser irradiation they found no significant melting up to lattice temperatures of ~1230 K, indicating that the particles maintained their integrity. Under continuous heating, however, they observed a shift of the longitudinal SPR at temperatures of ~40% of the melting point of the bulk metal caused by surface melting. This large difference between laser-induced heating and continuous heating was attributed to thermal diffusion to the environment of the rod: in the laser experiments the rods do not stay hot for long enough after excitation for significant structural changes to occur.

Gold nanorods constitute an attractive system to study melting in nanoscale objects. Their longitudinal SPR occurs away from the interband transitions in gold,[26] resulting in a narrow linewidth and an absorption cross section that can be an order of magnitude higher than that of a spherical particle of the same volume. In solution based studies it has been shown that femtosecond laser irradiation[29,50,51] depletes the population of nanorods which exhibit a non-zero absorption cross section at the laser illumination wavelength. When melted, the high energy geometry of the gold nanorod undergoes a shape transformation to the energetically more favored spherical geometry[29,50–52] through a migration of surface atoms.[20,53] Due to the sensitivity of the longitudinal SPR to the particle geometry,[2] this is accompanied by a drastic change in the absorption and scattering profile. Such laser-induced reshaping of non-spherical objects has been widely employed to narrow down the initially broad range of sizes and shapes in colloidal solutions of metal particles.[54–56]

Theoretical studies have predicted that the melting and reshaping of gold nanorods depend in unique ways on the size and aspect ratio.[40,57,58] Bouhelier *et al.* measured the angular photoluminescence of a single molten gold nanorod, but did not report a systematic study of the thermodynamic reshaping properties of the particle.[59] Other reports on the melting and reshaping of gold nanorods have so far only been conducted on ensembles.[29,49–52] In ensemble measurements however, the different dimensions of the individual particles are likely to screen any effects of size and aspect ratio, and large discrepancies between the calculated and the measured melting energy have been observed.[51] Recent advances in far-field microscopy have allowed for the detection and spectroscopy of single metal nanoparticles.[26,60–62] Studying a single nanorod removes the heterogeneity in the sample and allows one to study the size and shape effects of the melting transition. Here we study the melting and reshaping of single gold nanorods embedded in a polyvinyl alcohol matrix. We collected scattering spectra of individual gold nanorods before and after irradiation, and correlated these with electron microscope images. We found a melting energy which is in good agreement with theoretical predictions assuming thermodynamic values for bulk gold. We observed that higher aspect ratio particles are thermodynamically less stable, leading to a greater reduction of the aspect ratio at lower laser pulse energy densities.

Experimental

Gold nanorods were prepared using a wet-chemical synthesis method.[63] The rods have an ensemble average size of 92×30 nm, and an ensemble average volume of 5.8×10^4 nm^3. To ensure that the nanorods are in a homogeneous environment, we first spincoated a thin layer of polyvinyl alcohol (PVA) on an indium tin oxide (ITO) coated coverslip. A dilute solution of the nanorods was mixed with a 3% PVA solution, and spincoated onto the intial PVA layer. The sample was then sealed with another pure PVA layer identical to the first layer. With an atomic force microscope we measured the thickness of the individual layers to be 80 nm, 30 nm, and 80 nm, respectively. We fabricated grids in the PVA layer by femtosecond laser writing to help locate the same nanorods for spectroscopy and electron microscopy.

Single particle white-light scattering microscopy[60] was performed in a home built optical microscope (see Fig. 1). The output from a high power quartz tungsten halogen light source was spatially filtered using a 30 μm pinhole, and was focused onto the sample through a 1.4 NA oil immersed objective lens. The reflected light was collected by the same objective and directed to a photomultiplier tube (PMT, Oriel Instruments 77348). To increase the visibility of the rods, the reflected light was bandpass-filtered (760 ± 60 nm) before detection. The unfiltered scattering spectrum of each individual nanorod was dispersed by a spectrograph (Acton Instruments, SpectraPro 300i) on a charge coupled device (Princeton Instruments, PIXIS 100). Except for polarization measurements, the white light was randomly polarized.

To induce melting and reshaping, the nanorods were illuminated with a femtosecond pulse laser source (SpectraPhysics Tsunami, pulse width 100 fs, repetition rate 82 MHz, tunable 700–1000 nm). An electro-optic modulator (ConOptics Inc., 350–160) selected single pulses on demand from the 82 MHz pulse train. A half wave plate was used to rotate the polarization of the linear excitation source to match the orientation of the nanorod on the sample surface. Unless stated explicitly, all the nanorods were irradiated with a laser wavelength corresponding to the peak of their longitudinal SPR, and with a polarization parallel to the long axis of the nanorod.

In the white-light scattering measurements the measured intensity I_m at the detector is a superposition of the reflected

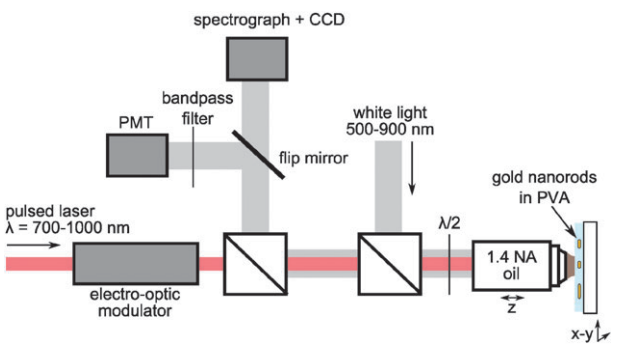

Fig. 1 Schematic drawing of the experimental setup used for white-light scattering spectroscopy and laser illumination of single gold nanoparticles.

field off the interface E_r and the light field E_s scattered by the particle:[60]

$$I_m(\lambda) = |E_r + E_s|^2. \quad (1)$$

The field at the detector is thus composed of a pure scattering signal, a signal due to the reflection of the interface, and component due to the interference between the reflected and scattered fields. The pure scattering signal scales as R^6 and is the dominant term for our large nanorods ($r_{eff} \sim 25$ nm). The detected intensity can then be expressed as

$$I_m(\lambda) = |E_i|^2[r^2 + |s(\lambda)|^2], \quad (2)$$

where the reflection term was included to correct for the weak reflection of the oil–polymer–glass interface. In the experiment, we correct for the reflection signal by subtracting a background spectrum I_{bg}, which was recorded several microns away from the particle. The spectral characteristics of the white light profile were taken into account by normalizing each spectrum to I_{WL}, which was recorded at the glass–air interface at the back of the coverslip. We then extracted the absolute scattering cross section σ_{sca} by taking into account the focal spot size A_{foc} and the collection efficiency ϕ of the setup using

$$\sigma_{sca}(\lambda) = \frac{A_{foc}}{\phi}\frac{I_m(\lambda) - I_{bg}(\lambda)}{I_{WL}(\lambda)}. \quad (3)$$

We note that this approach is only valid in an index matched geometry where $I_{bg}(\lambda)$ is much smaller than the scattered intensity. If this is not the case, the interference between the scattered and reflected waves should be included in eqn (2).[60]

To enable comparison between the individual nanorods, we applied several selection criteria before including each respective nanorod in our final analysis: (1) We only analyzed nanorods with a comparable area under the longitudinal SPR in the scattering spectrum (standard deviation 10%). Because the total scattered field scales as V^2, this selects a subpopulation with a standard deviation of 5% in volume. (2) We only considered nanorods with a peak value of $\sigma_{sca} = 1.55 \pm 0.2 \times 10^{-15}$ m^2 in randomly polarized light (standard deviation 12%). Because σ_{sca} scales as V^2 and σ_{abs} scales as V, this criterium isolates nanorods with a standard deviation of 5.8% in σ_{abs}. (3) We finally split the irradiated nanorods into two separate populations according to their longitudinal SPR energy, corresponding to average initial aspect ratios of 2.5 ± 0.2 (longitudinal SPR 750 ± 20 nm) and 3 ± 0.2 (longitudinal SPR 805 ± 15 nm).

Results and discussion

To locate the nanorods, the white light spot was raster scanned over the sample surface. We then acquired white light scattering spectra of the individual gold nanorods before irradiation. In Fig. 2 we show a selection of scattering spectra of individual gold nanorods in unpolarized white light. On the vertical axis in Fig. 2 we have plotted the absolute scattering cross section of the nanorods, σ_{sca}, extracted from eqn (3).

In the scattering spectra we observe a longitudinal SPR ranging from 1.4–1.7 eV (equivalent to 840–740 nm). The Lorentzian linewidth is $\Gamma = 105 \pm 20$ meV, which is in good

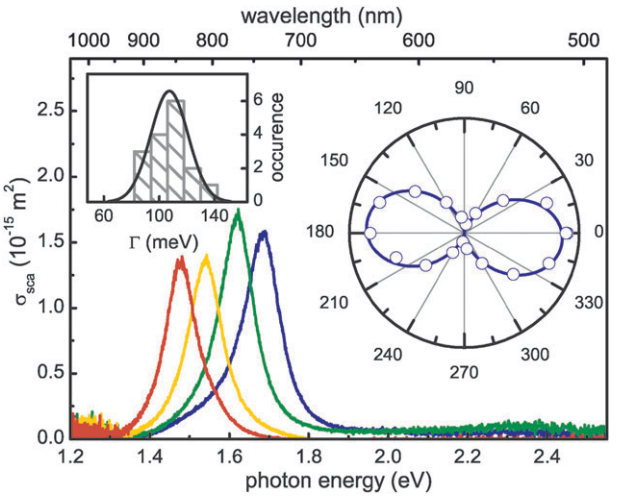

Fig. 2 Scattering spectrum of four individual gold nanorods in unpolarized white light. Inset: statistics of the Lorentzian linewidth and the polarized scattering *versus* angle, with a dipolar cosine fit (solid line).

agreement with previous reports.[62,64] In all cases, the polarized scattered intensity followed the expected dipolar angle dependence (see the inset in Fig. 2). These scattering spectra help us locate isolated gold nanorods, determine their orientation on the sample surface, and select the appropriate irradiation wavelength for each individual nanorod.

To establish a correlation between the physical and optical properties, we acquired the scattering spectrum and the scanning electron microscopy (SEM) image of ~20 nanorods. The correlation between aspect ratio and longitudinal SPR energy for all the particles is displayed in Fig. 3, together with two typical SEM images of nanorods with a different aspect ratio. As expected, we find a strong correlation between aspect ratio and longitudinal SPR energy. The small spread of the data points is caused by differences in the (effective) refractive index of the local environment around each nanorod, possibly caused by impurities or local air/water content in the polymer matrix. The dotted line in the figure indicates the calculated longitudinal SPR energy[65] for a spherically capped cylinder with a width of 30 nm, as reported by Prescott *et al.* We find good agreement between the calculated and measured SPR energy, indicating that the rods can be accurately modeled as spherically capped cylinders.

Individual gold nanorods were then irradiated with a single femtosecond laser pulse, which is shown in Fig. 4. In Fig. 4a we show σ_{sca} of a nanorod with an initial longitudinal SPR at 1.68 eV (745 nm). Using the correlation displayed in Fig. 3, we estimate the initial aspect ratio of the particle to be 2.5 ± 0.2 (we could not obtain SEM images of the rods before irradiation, because the electron beam induced damage to the PVA film made it impossible to obtain scattering spectra after electron microscope imaging). This rod was irradiated with a single laser pulse with a pulse energy density of 1.93 mJ cm^{-2} in the focal plane ($\lambda = 745$ nm). After irradiation, we find that the longitudinal SPR energy has blue-shifted to 1.96 eV (640 nm). We also observe a significant broadening of the longitudinal SPR, which is caused by the interband transitions

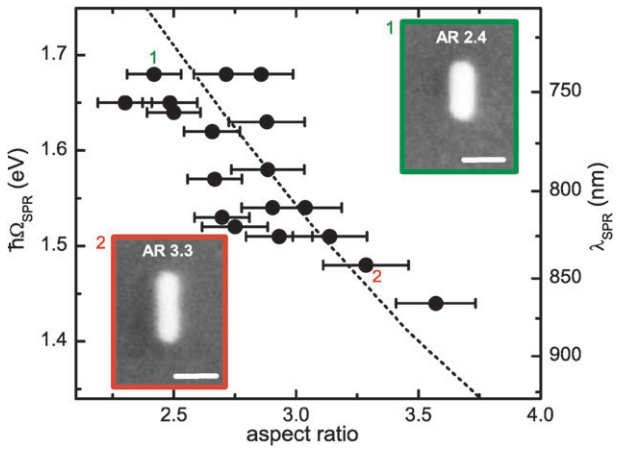

Fig. 3 Correlation between the aspect ratio (measured from SEM images of each rod) and the longitudinal SPR energy (measured from the scattering spectrum of each rod). The error bars indicate the uncertainty in the dimensions obtained from the SEM images. The dotted line is the calculated longitudinal SPR energy for spherically capped cylinders embedded in a medium with $\varepsilon_m = 2.25$ (see text for more details). Insets: scanning electron microscope images of two individual nanorods with a different aspect ratio. The scale bars are 50 nm.

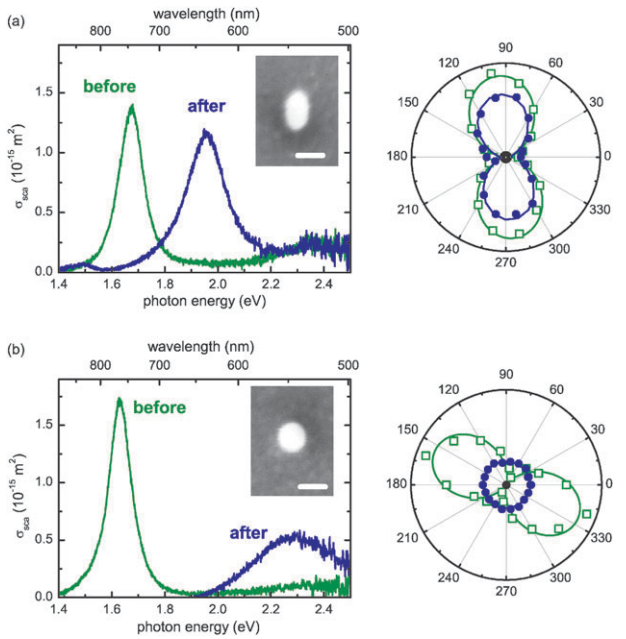

Fig. 4 Melting and reshaping single gold nanorods. (a) Scattering cross sections in unpolarized white light, before and after irradiation with a single laser pulse at 745 nm with an energy density of 1.93 mJ cm^{-2}. The polar plot shows polarized scattering *versus* angle before (squares) and after (circles) irradiation, with dipolar cosine fits (solid lines). Inset: SEM image of the nanorod after irradiation, scale bar 50 nm. (b) Same as (a), only this nanorod was irradiated with 2.5 mJ cm^{-2}.

in gold which have an onset energy of ~2 eV. The polarized scattered intensity did not change significantly from the initial particle due to the remaining elongated particle shape. From the SEM image acquired after irradiation we find that the aspect ratio of the particle was reduced from 2.5 to 1.6.

In Fig. 4b we show σ_{sca} for another gold nanorod (initial longitudinal SPR at 1.67 eV or 750 nm, aspect ratio 2.5 ± 0.2). We illuminated this rod with a higher pulse energy density of 2.5 mJ cm^{-2} (λ = 745 nm), upon which it completely relaxed to the spherical geometry. From the SEM image acquired after reshaping we observe a spherical particle with a radius of 24 nm. As expected, the scattering spectrum after irradiation displayed a peak at 2.3 eV (540 nm), corresponding to the sphere SPR. The initial dipole character of the polarized scattered intensity now displays a monopole character due to the loss of anisotropy in the particle shape.

As expected, upon melting the nanorods (partly) reshape to the energetically favored spherical geometry. The particle shape we observed for three different particles after irradiation with an increasing laser pulse energy is displayed in Fig. 5. The particles had an initial aspect ratio of 2.5 ± 0.2, and were illuminated with a laser wavelength on resonance with their longitudinal SPR peak. We observe a gradual shape change from a long nanorod to a shorter and wider nanorod, before the particle finally relaxes to the spherical shape.

We repeated the experiment displayed in Fig. 4 on approximately 20 nanorods which fall within the selection criteria outlined in the Experimental section. In Fig. 6 we show the longitudinal SPR after irradiation *versus* the amount of absorbed energy (corrected for laser spot size and objective transmission at the laser wavelength). We determined the amount of energy absorbed by a nanorod by considering the pulse energy density, I, in the focal plane, and the absorption cross section σ_{abs}^{avg}, where the superscript indicates that the value is averaged over the narrow sub-population we considered. The amount of energy absorbed by the rod can then be expressed as $Q_{abs} = I \times \sigma_{abs}^{avg}$. We obtain an estimate for σ_{abs}^{avg} from the theoretical ratio between the scattering and absorption cross section. We calculated this ratio in the electrostatic approach, for which we employed Gans' theory[66] with the estimated shape factors L reported by Prescott *et al.*[65] for a spherically capped cylinder with a width of 30 nm. Using typical parameters for our nanorods embedded in PVA with

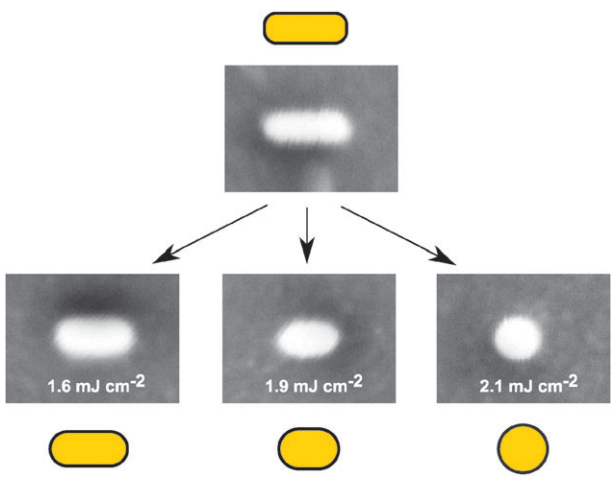

Fig. 5 Sketch of the intermediate particle shapes observed at different pulse energy densities. The dimensions of all SEM images are 200 × 150 nm.

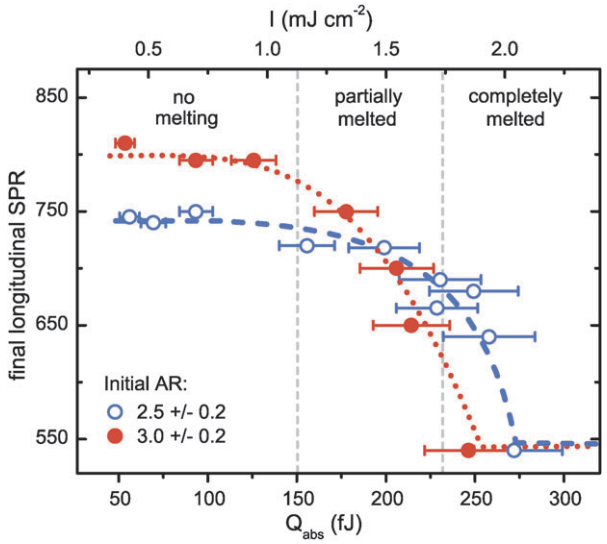

Fig. 6 Dependence of the longitudinal SPR energy after irradiation on the amount of absorbed laser energy, for two populations with an initial aspect ratio of 2.5 ± 0.2 (solid symbols) and 3.0 ± 0.2 (open symbols). The errors indicate the uncertainty in the amount of absorbed energy (s.d.), see the text for details. The lines are a guide to the eye. The vertical dashed lines indicate the calculated energy range associated with no melting ($T < 1330$ K), partial melting ($T = 1330$ K), and full melting ($T > 1330$ K).

an aspect ratio of 2.7 we find $\sigma_{abs}^{avg}/\sigma_{sca}^{avg} = 4.3$. The expression relating Q_{abs} and I is then

$$Q_{abs} = 4.3 \times I \times \sigma_{sca}^{avg}. \quad (4)$$

The relative error entailed in this approach is largely determined by the relative error in σ_{sca}^{avg}, which is twofold. Firstly, our approximation to neglect the interference term in eqn (1) introduces an error determined by the measured value of $r^2/|s|^2 = 0.08$. Secondly, our averaging over an ensemble with a standard deviation of 12% in σ_{sca} introduces an additional error. We estimate the total error in Q_{abs} to be approximately 20%.

From Fig. 6 we find that both aspect ratios require ~260 fJ to completely relax to the spherical geometry. From thermodynamic considerations we can express the amount of energy required to just melt a nanorod as[67]

$$Q_{melt} = \rho V[c_p(T_{melt} - T_0) + \Delta H_{fus}], \quad (5)$$

where ρ is the density of bulk gold, V is the volume of the nanorod, c_p is the specific heat capacity of bulk gold[37] (129 J kg^{-1} K^{-1}), T_{melt} is the melting temperature of bulk gold[37] (1330 K), T_0 is the ambient temperature, and ΔH_{fus} is the heat of fusion for bulk gold[37] (6.5×10^4 J kg^{-1}). Employing the ensemble average volume of 5.8×10^4 nm^3 we find $Q_{melt} = 225 \pm 15$ fJ for a typical nanorod in our experiment (the error originates from the uncertainty in the typical volume of the rods of 4.8%, see the Experimental section). In our experiment we find a melting energy which is ≈15% larger than the theoretical prediction. This could be due to the viscoelasticity of the polymer matrix, which counters the surface energy driven migration of the molten gold atoms to form a spherical particle. This is expected to increase the amount of energy required for structural changes to occur. Also effects of the cooling of the particle during reshaping could contribute to the observed discrepancy. Ruan *et al.* reported that a gold sphere undergoes full melting within 100 ps.[42] In combination with an estimated 1 ns cooling time,[68] this implies that approximately 10% of the heat has dissipated before melting, which may explain the difference between the measured and calculated melting energies.

The initial stages of the reshaping at energies below ≈200 fJ exhibit a gradual structural change into shorter aspect ratio particles. In this pulse energy regime the nanorod undergoes partial melting, and only a thin shell of surface atoms migrates to form a lower energy geometry. When the nanorod absorbed more than ≈220 fJ, the particles suddenly collapsed to a spherical geometry. This behavior is similar to previous molecular dynamics studies performed by Wang *et al.*, who modeled the melting and reshaping of a small, freestanding gold nanorod.[40] The authors simulated the continuous heating of gold nanorods from 5–1300 K, and analyzed the equilibrium atomic structure at different temperatures. They reported that the nanorods initially undergo a gradual shape transition to a shorter and wider particle. Around the bulk melting point the internal atomic structure of the nanorod suddenly became disordered and the nanorod collapsed to the spherical geometry, which is similar to the behavior we observe in our experiment.

Their simulations also indicated the formation of an intermediate, stable particle with a lower aspect ratio. This intermediate shape was the result of a surface reorganization from {110} and {100} facets to the energetically more stable {111} facets.[40,57,58] The intermediate product covered with {111} facets was found to be stable up to the bulk melting point of gold. The temperature at which this intermediate geometry occurred was found to increase with increasing particle size and approached the homogeneous melting temperature for large systems. As a consequence, the intermediate stable particle shape was precluded in large nanorods, which is probably why we do not observe this in our experiment.

Interestingly, we find that partial structural changes occur at a lower pulse energy density for longer aspect ratio particles. For example, for $Q_{abs} \approx 220$ fJ, the particles with an initial aspect ratio of 3 underwent significant structural changes to an aspect ratio of ~1.8, but the particles with an initial aspect ratio of 2.5 were hardly affected, exhibiting an aspect ratio of ~2.2. Because of our selection criteria outlined in the Experimental section, this effect cannot be caused by differences in particle volume or absorption cross section. We suggest that the observed difference in energy required for reshaping is due to the difference in surface energy between the two aspect ratios. The shape of the particle after laser induced heating is driven by the tendency of surfaces to reduce their surface energy. Surface energy being proportional to surface area, the total surface energy difference, relative to the lowest energy geometry of a sphere, is almost 20% larger for an aspect ratio of 3 compared to an aspect ratio of 2.5 (assuming a constant volume). Due to this difference in surface energy, an aspect ratio 3 particle may exhibit a higher rate of reshaping in order to minimize its surface energy. The homogeneous melting temperature still occurs at a similar

temperature for both aspect ratios because this is determined by the bulk melting temperature of gold.

Conclusion

We have studied the melting and reshaping of single gold nanorods using a combination of white-light scattering spectroscopy and electron microscopy. We measured a melting energy of 260 fJ for nanorods with an average size of 92 × 30 nm, which is in good agreement with the theoretical value of 225 fJ. We observed that higher aspect ratio particles are thermodynamically less stable, leading to a greater reduction in aspect ratio upon partial melting. Our technique is capable of accurately determining the melting energy of individual nanoscale objects, which can give valuable insight in size and shape effects on the melting transition. Accurate knowledge about the melting threshold should also prove useful to photothermal applications of gold nanorods, where shape transitions need to be limited or prevented altogether.

References

1 P. Mulvaney, *Langmuir*, 1996, **12**, 788–800.
2 K. L. Kelly, E. Coronado, L. L. Zhao and G. C. Schatz, *J. Phys. Chem. B*, 2003, **107**, 668–677.
3 P. K. Jain, K. S. Lee, I. H. El-Sayed and M. A. El-Sayed, *J. Phys. Chem. B*, 2006, **110**, 7238–7248.
4 M. Valden, X. Lai and D. W. Goodman, *Science*, 1998, **281**, 1647–1650.
5 R. M. Crooks, M. Q. Zhao, L. Sun, V. Chechik and L. K. Yeung, *Acc. Chem. Res.*, 2001, **34**, 181–190.
6 S. A. Maier, M. L. Brongersma, P. G. Kik, S. Meltzer, A. A. G. Requicha and H. A. Atwater, *Adv. Mater.*, 2001, **13**, 1501–1505.
7 W. L. Barnes, A. Dereux and T. W. Ebbesen, *Nature*, 2003, **424**, 824–830.
8 D. E. Chang, A. S. Sørensen, E. A. Demler and M. D. Lukin, *Nature Phys.*, 2007, **3**, 807–812.
9 P. Ghenuche, S. Cherukulappurath, T. H. Taminiau, N. F. van Hulst and R. Quidant, *Phys. Rev. Lett.*, 2008, **101**, 116805.
10 K. Kneipp, Y. Wang, H. Kneipp, L. T. Perelman, I. Itzkan, R. Dasari and M. S. Feld, *Phys. Rev. Lett.*, 1997, **78**, 1667–1670.
11 A. M. Michaels, M. Nirmal and L. E. Brus, *J. Am. Chem. Soc.*, 1999, **121**, 9932–9939.
12 A. D. McFarland and R. P. van Duyne, *Nano Lett.*, 2003, **3**, 1057–1062.
13 H. F. Wang, T. B. Huff, D. A. Zweifel, W. He, P. S. Low, A. Wei and J. X. Cheng, *Proc. Natl. Acad. Sci. U. S. A.*, 2005, **102**, 15752–15756.
14 C. Sönnichsen, B. M. Reinhard, J. Liphardt and A. P. Alivisatos, *Nat. Biotechnol.*, 2005, **23**, 741–745.
15 N. J. Durr, T. Larson, D. K. Smith, B. A. Korgel, K. Sokolov and A. Ben-Yakar, *Nano Lett.*, 2007, **7**, 941–945.
16 C. Yu, H. Nakshatri and J. Irudayaraj, *Nano Lett.*, 2007, **7**, 2300–2306.
17 J. W. Stone, P. N. Sisco, E. C. Goldsmith, S. C. Baxter and C. J. Murphy, *Nano Lett.*, 2007, **7**, 116–119.
18 C. L. Baciu, J. Becker, A. Janshoff and C. Sönnichsen, *Nano Lett.*, 2008, **8**, 1724–1728.
19 M. Sugiyama, S. Inasawa, S. Koda, T. Hirose, T. Yonekawa, T. Omatsu and A. Takami, *Appl. Phys. Lett.*, 2001, **79**, 1528–1530.
20 J. Pérez-Juste, B. Rodríguez-González, P. Mulvaney and L. M. Liz-Marzán, *Adv. Funct. Mater.*, 2005, **15**, 1065–1071.
21 J. W. M. Chon, C. Bullen, P. Zijlstra and M. Gu, *Adv. Funct. Mater.*, 2007, **17**, 875–880.
22 P. Zijlstra, J. W. M. Chon and M. Gu, *Nature*, 2009, **459**, 410–413.
23 L. R. Hirsch, R. J. Stafford, J. A. Bankson, S. R. Sershen, B. Rivera, R. E. Price, J. D. Hazle, N. J. Halas and J. L. West, *Proc. Natl. Acad. Sci. U. S. A.*, 2003, **100**, 13549–13554.
24 X. H. Huang, I. H. El-Sayed, W. Qian and M. A. El-Sayed, *J. Am. Chem. Soc.*, 2006, **128**, 2115–2120.
25 J. L. Li, D. Day and M. Gu, *Adv. Mater.*, 2008, **20**, 3866–3871.
26 C. Sönnichsen, T. Franzl, T. Wilk, G. von Plessen, J. Feldmann, O. Wilson and P. Mulvaney, *Phys. Rev. Lett.*, 2002, **88**, 077402.
27 H. Inouye, K. Tanaka, I. Tanahashi and K. Hirao, *Phys. Rev. B*, 1998, **57**, 11334–11340.
28 M. Hu and G. V. Hartland, *J. Phys. Chem. B*, 2002, **106**, 7029–7033.
29 S. Link, C. Burda, B. Nikoobakht and M. A. El-Sayed, *J. Phys. Chem. B*, 2000, **104**, 6152–6163.
30 J. R. Sambles, *Proc. R. Soc. London, Ser. A*, 1971, **324**, 339–351.
31 P. Buffat and J. P. Borel, *Phys. Rev. A*, 1976, **13**, 2287–2298.
32 F. Ercolessi, W. Andreoni and E. Tosatti, *Phys. Rev. Lett.*, 1991, **66**, 911–914.
33 A. N. Goldstein, C. M. Echer and A. P. Alivisatos, *Science*, 1992, **256**, 1425–1427.
34 S. L. Lai, J. Y. Guo, V. Petrova, G. Ramanath and L. H. Allen, *Phys. Rev. Lett.*, 1996, **77**, 99–102.
35 K. Dick, T. Dhanasekaran, Z. Y. Zhang and D. Meisel, *J. Am. Chem. Soc.*, 2002, **124**, 2312–2317.
36 S. Inasawa, M. Sugiyama and Y. Yamaguchi, *J. Phys. Chem. B*, 2005, **109**, 3104–3111.
37 R. C. Weast and D. R. Lide, *CRC Handbook of Chemistry and Physics*, CRC press, Boca Raton, Florida, 85th edn, 2004.
38 S. Williamson, G. Mourou and J. C. M. Li, *Phys. Rev. Lett.*, 1984, **52**, 2364–2367.
39 C. Guo, G. Rodriguez, A. Lobad and A. J. Taylor, *Phys. Rev. Lett.*, 2000, **84**, 4493–4496.
40 Y. T. Wang and C. Dellago, *J. Phys. Chem. B*, 2003, **107**, 9214–9219.
41 B. J. Siwick, J. R. Dwyer, R. E. Jordan and R. J. D. Miller, *Science*, 2003, **302**, 1382–1385.
42 C. Y. Ruan, Y. Murooka, R. K. Raman and R. A. Murdick, *Nano Lett.*, 2007, **7**, 1290–1296.
43 R. Ernstorfer, M. Harb, C. T. Hebeisen, G. Sciaini, T. Dartigalongue and R. J. D. Miller, *Science*, 2009, **323**, 1033–1037.
44 A. Plech, V. Kotaidis, S. Grésillon, C. Dahmen and G. von Plessen, *Phys. Rev. B*, 2004, **70**, 195423.
45 R. Kofman, P. Cheyssac, A. Aouaj, Y. Lereah, G. Deutscher, T. Bendavid, J. M. Penisson and A. Bourret, *Surf. Sci.*, 1994, **303**, 231–246.
46 N. Combe, P. Jensen and A. Pimpinelli, *Phys. Rev. Lett.*, 2000, **85**, 110–113.
47 G. V. Hartland, M. Hu and J. E. Sader, *J. Phys. Chem. B*, 2003, **107**, 7472–7478.
48 A. Plech, R. Cerna, V. Kotaidis, F. Hudert, A. Bartels and T. Dekorsy, *Nano Lett.*, 2007, **7**, 1026–1031.
49 H. Petrova, J. Pérez-Juste, I. Pastoriza-Santos, G. V. Hartland, L. M. Liz-Marzán and P. Mulvaney, *Phys. Chem. Chem. Phys.*, 2006, **8**, 814–821.
50 S. S. Chang, C. W. Shih, C. D. Chen, W. C. Lai and C. R. C. Wang, *Langmuir*, 1999, **15**, 701–709.
51 S. Link and M. A. El-Sayed, *J. Chem. Phys.*, 2001, **114**, 2362–2368.
52 M. B. Mohamed, K. Z. Ismail, S. Link and M. A. El-Sayed, *J. Phys. Chem. B*, 1998, **102**, 9370–9374.
53 S. Link, Z. L. Wang and M. A. El-Sayed, *J. Phys. Chem. B*, 2000, **104**, 7867–7870.
54 H. Kurita, A. Takami and S. Koda, *Appl. Phys. Lett.*, 1998, **72**, 789–791.
55 J. Bosbach, D. Martin, F. Stietz, T. Wenzel and F. Träger, *Appl. Phys. Lett.*, 1999, **74**, 2605–2607.
56 S. Besner, A. V. Kabashin and M. Meunier, *Appl. Phys. Lett.*, 2006, **89**, 233122.
57 J. K. Diao, K. Gall and M. L. Dunn, *Phys. Rev. B*, 2004, **70**, 075413.
58 Y. T. Wang, S. Teitel and C. Dellago, *Nano Lett.*, 2005, **5**, 2174–2178.
59 A. Bouhelier, R. Bachelot, G. Lerondel, S. Kostcheev, P. Royer and G. P. Wiederrecht, *Phys. Rev. Lett.*, 2005, **95**, 267405.
60 K. Lindfors, T. Kalkbrenner, P. Stoller and V. Sandoghdar, *Phys. Rev. Lett.*, 2004, **93**, 037401.
61 M. A. van Dijk, M. Lippitz and M. Orrit, *Acc. Chem. Res.*, 2005, **38**, 594–601.

62 P. Zijlstra, A. L. Tchebotareva, J. W. M. Chon, M. Gu and M. Orrit, *Nano Lett*., 2008, **8**, 3493–3497.
63 B. Nikoobakht and M. A. El-Sayed, *Chem. Mater*., 2003, **15**, 1957–1962.
64 C. Novo, D. Gomez, J. Pérez-Juste, Z. Y. Zhang, H. Petrova, M. Reismann, P. Mulvaney and G. V. Hartland, *Phys. Chem. Chem. Phys*., 2006, **8**, 3540–3546.
65 S. W. Prescott and P. Mulvaney, *J. Appl. Phys*., 2006, **99**, 123504.
66 C. F. Bohren and D. R. Huffman, *Absorption and Scattering of Light by Small Particles*, John Wiley & Sons. Inc., New York, 1998.
67 A. Bejan, *Heat Transfer*, John Wiley & Sons, Inc., New York, 1993.
68 F. Cooper, *Int. J. Heat Mass Transfer*, 1977, 991–993.